Imaging the Phase of an Evolving Bose-Einstein Condensate Wave Function

J. E. Simsarian,[1] J. Denschlag,[1] Mark Edwards,[1,2] Charles W. Clark,[1] L. Deng,[1]
E. W. Hagley,[1] K. Helmerson,[1] S. L. Rolston,[1] and W. D. Phillips[1]
[1]*National Institute of Standards and Technology, Gaithersburg, Maryland 20899*
[2]*Georgia Southern University, Statesboro, Georgia 30460-8031*
(Received 28 April 2000)

We demonstrate a spatially resolved autocorrelation measurement with a Bose-Einstein condensate and measure the evolution of the spatial profile of its quantum mechanical phase. Upon release of the condensate from the magnetic trap, its phase develops a form that we measure to be quadratic in the spatial coordinate. Our experiments also reveal the effects of the repulsive interaction between two overlapping condensate wave packets and we measure the small momentum they impart to each other.

PACS numbers: 03.75.Fi, 32.80.Qk, 39.20.+q

A trapped Bose-Einstein condensate (BEC) [1] has unique value as a source for atom lasers [2] and matter-wave interferometry [3] because its atoms occupy the same quantum state, with uniform spatial phase. However, when released from the trapping potential, a BEC with repulsive atom-atom interactions expands, developing a nonuniform phase profile. Understanding this phase evolution will be important for applications of coherent matter waves. We have developed a new interferometric technique using spatially resolved autocorrelation to measure the functional form and time evolution of the phase of a BEC wave packet expanding under the influence of its mean-field repulsion.

In 1997, the coherence of weakly interacting BECs was demonstrated by releasing two spatially separated condensates and observing their interference [4]. Subsequent experiments have further investigated condensate coherence properties. One [5] used velocity-resolved Bragg diffraction [6] to probe the momentum spectrum of trapped and released BECs. A complementary experiment [7] that used matter-wave interferometry can be interpreted as a measurement of the spatial correlation function, whose Fourier transform is the momentum spectrum. These experiments showed that a trapped condensate has a uniform phase, and a released condensate develops a nonuniform phase profile. (Recently the influence of nonzero temperature on coherence properties was also investigated [8].) The experiments reported in this Letter combine spatial resolution and interferometry to measure the functional form of the time-dependent phase profile of a released condensate. We also make the first measurement of the velocity imparted to two equal BEC wave packets from their mutual mean-field repulsion [9].

We perform our experiments with a condensate of $1.8(4) \times 10^6$ [10] sodium atoms in the $3S_{1/2}$, $F = 1$, $m_F = -1$ state. The sample has no discernible noncondensed (i.e., thermal) component. The condensate is prepared following the method of Ref. [6] and is held in a magnetic trap with trapping frequencies $\omega_x = \sqrt{2}\,\omega_y = 2\omega_z = 2\pi \times 27$ Hz. Using a scattering length of $a =$ 2.8 nm, the calculated Thomas-Fermi diameters [11] are 47, 66, and 94 μm, respectively.

We release the BEC from the magnetic trap and it expands, driven mostly by the mean-field repulsion of the atoms. This expansion implies the development of a nonuniform spatial phase profile (recall that the velocity field is proportional to the gradient of the quantum phase). After an expansion time T_0, we probe the phase profile with matter-wave Bragg interferometry [12–14]. Our interferometer splits the BEC into two wave packets and recombines them with a chosen overlap, producing interference fringes, which we measure with absorption imaging [15]. From the dependence of the fringe spacing on the overlap, we extract the phase profile of the wave packets.

Our atom interferometer [14] consists of three optically induced Bragg-diffraction pulses applied successively in time (Fig. 1). Each pulse consists of two counterpropagating laser beams whose frequencies differ by 100 kHz. They are detuned by about -2 GHz from atomic resonance ($\lambda = 2\pi/k = 589$ nm) so that spontaneous emission is negligible. The first pulse has a duration of 6 μs

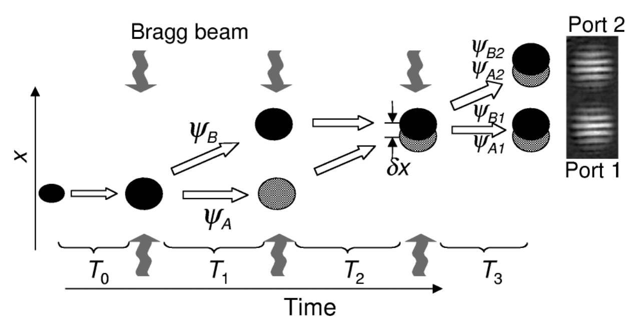

FIG. 1. Space-time diagram of the experiment. Three optically induced Bragg-diffraction pulses form the interferometer. The condensate is released for a time T_0 before the first Bragg pulse. The centers of ψ_A and ψ_B are separated by δx at the time of the third Bragg pulse, which splits them into ψ_{A1}, ψ_{B1}, and ψ_{A2}, ψ_{B2}. Before imaging the atoms, we allow the output ports to separate for a time $T_3 \approx 2$ ms. The image shows the output ports when $T_0 = 3$ ms, $T_1 = 1$ ms, and $T_2 = 1.3$ ms.

 0031-9007/00/85(10)/2040(4)$15.00

and intensity sufficient to provide a $\pi/2$ pulse, which coherently splits the BEC into two wave packets, ψ_A and ψ_B. The wave packets have about the same number of atoms and differ only in their momenta: $p = 0$ and $p = 2\hbar k$. At a time $T_1 = 1$ ms after the first Bragg pulse, the two wave packets are completely separated and a second Bragg pulse (a π pulse) of 12 μs duration transfers ψ_B to a state with $p \approx 0$ and ψ_A to $p \approx 2\hbar k$ [16]. After a variable time T_2 the wave packets partially overlap again and we apply a third pulse, of 6 μs duration (a $\pi/2$ pulse). This last pulse splits each wave packet into the two momentum states. The interference of the overlapping wave packets in each of the two momentum states allows the determination of the local phase difference between them. By changing the time T_2 we vary $\delta x = x_A - x_B$, the separation of ψ_A and ψ_B at the time of the final Bragg pulse. The set of data at different δx constitutes a new type of spatial autocorrelation measurement that is similar to the "FROG" technique [17] used to measure the complete electric field of ultrafast laser pulses. From these measurements we obtain the phase profile of the wave packets in the x direction.

Figures 2a–2e shows one interferometer output port for different δx (different T_2) after an expansion time $T_0 = 4$ ms. In general, we observe straight, evenly spaced fringes (although for small T_0 and T_2 the fringes may be somewhat curved). There is a value of $\delta x = x_0 \neq 0$ where we observe no fringes (Fig. 2c) and the fringe spacing decreases as $|\delta x - x_0|$ increases. Figure 2f, a cut through Fig. 2d, shows the high-contrast fringes [18]. Our data analysis uses the average fringe period d, obtained from plots like Fig. 2f.

The fringes come from two different effects: the interference of two wave packets with quadratic phase profile, and a relative velocity between the wave packets' centers. The data can be understood by calculating the fringe spacing along x at output port 1 [19]. We assume that the phase ϕ of the wave function $fe^{i\phi}$ can be written as $\phi = \frac{\alpha}{2}x^2 + \beta x$. The equal spacing of the fringes implies, as predicted in the Thomas-Fermi limit [20], that ϕ has no significant higher-order terms [21]. The curvature coefficient α describes the mean-field expansion of the wave packets and β describes a relative repulsion velocity. The velocity arises because the wave packets experience a repulsive push as they first separate and again as they recombine. The density at port 1 (see Fig. 1) just after the final interferometer pulse is the interference pattern $|\psi_{A1} + \psi_{B1}|^2$ of the wave packets ψ_{A1} and ψ_{B1}:

$$|f(x - \delta x)e^{i[(\alpha/2)(x-\delta x)^2 - \beta(x-\delta x)]} + f(x)e^{i[(\alpha/2)x^2+\beta x]}|^2, \tag{1}$$

where we assume that the amplitudes and curvatures of the wave packets are equal and their velocities have equal magnitude and opposite direction. The cross term of (1) is

$$2f(x - \delta x)f(x)\cos\left[\left(\alpha\,\delta x + \frac{M\,\delta v}{\hbar}\right)x + C\right], \tag{2}$$

where M is the sodium mass, $M\,\delta v/\hbar \equiv 2\beta$, and C is independent of x [22]. $\delta v = v_B - v_A$ is the relative repulsion velocity between the wave packets ψ_{A1} and ψ_{B1}. Expression (2) predicts fringes with spatial frequency,

$$\kappa = \alpha\,\delta x + \frac{M\,\delta v}{\hbar}, \tag{3}$$

where $|\kappa| = 2\pi/d$. When there are no fringes, $\kappa = 0$ and the wave packet separation $\delta x = x_0 \equiv -M\,\delta v/\alpha\hbar$.

Figure 3 plots the measured κ vs δx [23] for $T_0 =$ 1 and 4 ms. The data are well fit by a straight line as expected from Eq. (3) in the approximation that α and δv are independent of δx. The slopes of the lines are the phase curvatures α, and the κ intercepts give the relative velocities δv.

We checked the validity of the data analysis procedure by analyzing data simulated with a 1D Gross-Pitaevskii (GP) treatment. Despite variations of δv and α with δx (due to their continued evolution during the variable time T_2), we find that κ is still linear in δx. The slopes and intercepts in general are averages over the range of δx used in the experiment.

The interference fringes used to determine α and δv are created at the time of the final interferometer pulse. Because the two outputs overlap at that moment, we wait a time T_3 for them to separate before imaging. During

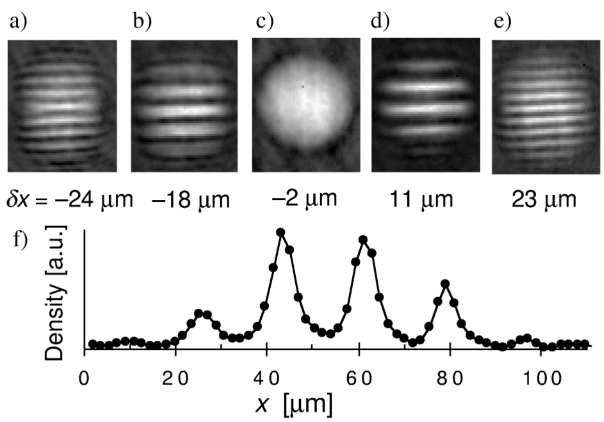

FIG. 2. (a)–(e) One of the two output ports of the interferometer with $T_0 = 4$ ms and δx as indicated. (f) A plot of the density along the x direction of (d).

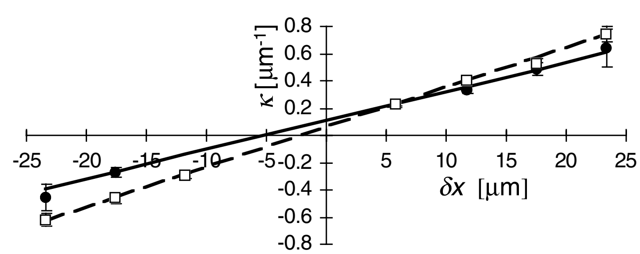

FIG. 3. Plot of the spatial fringe frequency κ versus δx for $T_0 = 1$ ms (filled circles) and 4 ms (open squares). The solid and dashed lines are linear fits to the data.

this time, the wave packets continue to expand. The 1D simulations show that the fringe spacings and the wave packets expand in the same proportion. We correct κ (by typically 15%) for this, using the calculated expansion from a 3D solution of the GP equation described below.

The different slopes and intercepts of the two lines in Fig. 3 show that the curvature α and relative velocity δv of the wave packets depend on the release time T_0 before the first interferometer pulse. Figure 4 plots the dependence of α and δv on various release times T_0. The condensate initially has a uniform phase so that immediately after its release from the trap $\alpha = 0$. We nevertheless measure a nonzero α for $T_0 = 0$ ms because the BEC expands during T_1 and T_2. As a function of time, α behaves as $\dot{D}/D$ where D is the wave packet diameter and $\dot{D}$ is its rate of change [20]. At early times when the mean-field energy is being converted to kinetic energy, $\dot{D}$ increases rapidly, *increasing* α. At late times, after the mean-field energy has been converted, D increases while $\dot{D}$ is nearly constant, *decreasing* α.

We predict the time evolution of α using the Lagrangian variational method (LVM) [24]. The LVM uses trial wave functions with time-dependent parameters to provide approximate solutions of the 3D time-dependent GP equation. In the model, the effect of the interferometer pulses is to replace the original wave packet with a superposition of wave packets having different momenta; e.g., the action of our first interferometer pulse is $\psi_0 \rightarrow (\psi_0 + e^{i2kx}\psi_0)/\sqrt{2}$. We use Gaussian trial wave functions in the LVM to calculate the phase curvature α at the time of the last interferometer pulse. For simplicity, the interaction between the wave packets is neglected. This result, with $T_1 = T_2$, is the solid line of Fig. 4a.

We use energy conservation to calculate the relative repulsion velocity δv between ψ_{A1} and ψ_{B1} because we neglect wave packet interactions in the LVM. In the Thomas-Fermi approximation, we can calculate the amount of energy available for repulsion when $T_0 = 0$. A trapped condensate has $\frac{5}{7}\mu$ average total energy per particle, where μ is the chemical potential [11]. After release from the trap, it has $\frac{2}{7}\mu$ average mean-field energy per particle. Applying a $\pi/2$ Bragg pulse to the BEC causes a density corrugation, which increases the mean-field energy to $\frac{3}{7}\mu$ per particle. In the approximation that the wave packets do not deform as they separate and recombine, one can show that $\frac{1}{3}$ of the total mean-field energy goes into expansion of the wave packets, and $\frac{2}{3}$ is available for kinetic energy of center-of-mass motion. Therefore $\frac{2}{7}\mu$ of mean-field energy per particle is available for repulsion. The corresponding repulsion velocity is only about 10^{-2} of a photon recoil velocity. The repulsion energy and δv decrease for larger T_0 because both are inversely proportional to the condensate volume, which we calculate with the LVM. The two curves shown in Fig. 4b are the calculated δv when $\delta x = 0$ (solid curve) and δv averaged over the different δx used in the experiment (dashed curve). The 1D GP simulations suggest that for small T_0, the results of the experiment should be closer to the solid curve, and for large T_0, closer to the dashed curve. The data are consistent with this trend.

In a related set of experiments we performed interferometry in the trap. This differs from the experiments on a released BEC because there is no expansion before the first interferometer pulse [25] and the magnetic trap changes the relative velocity of the wave packets between the interferometer pulses (Fig. 5a). To better reveal the velocity differences, we choose $T_1 = T_2 = T$ to suppress fringes arising from the phase curvature. As with the released BEC measurements, we observe equally spaced fringes at the output of the interferometer, although the fringes are almost entirely due to a relative velocity v between the wave packets ψ_{A1} and ψ_{B1} at the time of the third interferometer pulse. We obtain v from the fringe periodicity after a small correction for residual phase curvature [26].

Two effects contribute to v: the mutual repulsion between the wave packets ψ_A and ψ_B and the different action of the trapping potential on the two wave packets in the interferometer. The latter effect occurs because after the first Bragg pulse, ψ_A remains at the minimum of the magnetic potential while ψ_B is displaced. Wave packet ψ_B therefore

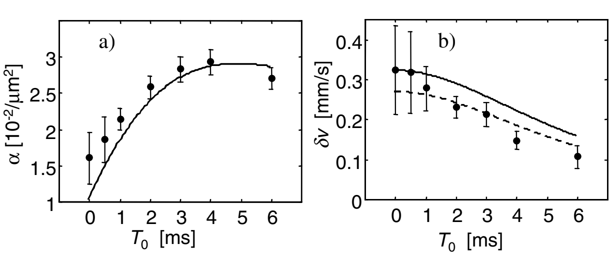

FIG. 4. (a) Plot of the phase curvature α versus the initial expansion time T_0 showing the phase evolution from mean-field expansion. The solid line is a calculation using the Lagrangian variational method (LVM). (b) Plot of the relative repulsion velocity δv versus T_0. The solid curve is the calculated maximum repulsion velocity (when $\delta x = 0$) and the dashed curve is the repulsion velocity averaged over the range of δx used in the experiment.

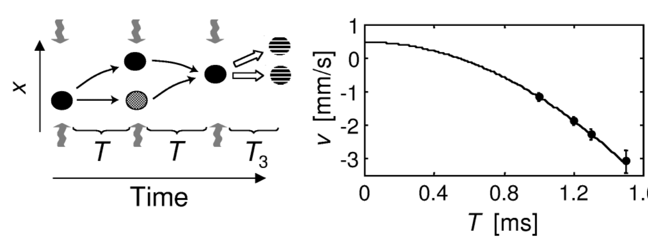

FIG. 5. (a) Schematic representation of the interferometer in the trap, with the principle difference from Fig. 1 being the curved arrows indicating the acceleration of the wave packets. (b) The relative velocity v between the two trapped wave packets versus the interferometer time T. The solid line is a fit.

spends more time away from the center of the trap and experiences more acceleration than ψ_A.

Following the last Bragg pulse, ψ_{A1} and ψ_{B1} have a velocity difference which for our parameters can be approximated by $v \approx -\frac{2\hbar k}{M}\sin^2(\omega_x T) + \delta v$ [27]. Figure 5b plots v versus T, and the curve is a fit to the above expression. We obtain the trap frequency $\omega_x/2\pi = 26.7(15)$ Hz, in excellent agreement with an independent measurement. We also obtain the relative velocity from the mean-field repulsion $\delta v = 0.49(12)$ mm/s, which we expect to be somewhat larger than for the released measurements because the wave packets contract, producing a larger mean field.

In conclusion, we demonstrate an autocorrelating matter-wave interferometer and use it to study the evolution of a BEC phase profile by analyzing spatial images of interference patterns. We study how the phase curvature of the condensate develops in time and measure the repulsion velocity between two BEC wave packets. Our interferometric method should be useful for characterizing other interesting condensate phase profiles. For example, it can be applied to detect excitations of a BEC with characteristic phase patterns, such as vortices and solitons [14,28–31]. The method should be useful for further studies of the interaction of coherent wave packets and to study the coherence of atom lasers.

We thank T. Busch, D. Feder, and L. Collins for helpful discussions. This work was supported in part by the U.S. Office of Naval Research and NASA. J. D. acknowledges support from the Alexander von Humboldt Foundation. M. E. and C. W. C. acknowledge partial support from NSF Grants No. 9802547 and No. 9803377.

[1] M. H. Anderson *et al.,* Science **269**, 198 (1995); K. B. Davis *et al.,* Phys. Rev. Lett. **75**, 3969 (1995); C. C. Bradley, C. A. Sackett, and R. G. Hulet, Phys. Rev. Lett. **78**, 985 (1997); see also C. C. Bradley *et al.,* Phys. Rev. Lett. **75**, 1687 (1995).

[2] M.-O. Mewes *et al.,* Phys. Rev. Lett. **78**, 582 (1997); E. W. Hagley *et al.,* Science **283**, 1706 (1999); I. Bloch, T. W. Hänsch, and T. Esslinger, Phys. Rev. Lett. **82**, 3008 (1999); B. P. Anderson and M. A. Kasevich, Science **282**, 1686 (1998).

[3] *Atom Interferometry,* edited by P. R. Berman (Academic Press, Cambridge, 1997).

[4] M. R. Andrews *et al.,* Science **275**, 637 (1997).

[5] J. Stenger *et al.,* Phys. Rev. Lett. **82**, 4569 (1999).

[6] M. Kozuma *et al.,* Phys. Rev. Lett. **82**, 871 (1999).

[7] E. W. Hagley *et al.,* Phys. Rev. Lett. **83**, 3112 (1999); M. Trippenbach *et al.,* J. Phys. B **33**, 47 (2000).

[8] I. Bloch, T. W. Hänsch, and T. Esslinger, Nature (London) **403**, 166 (2000).

[9] The mean-field energy shift of the out-coupled wave packet in [5] can be used to infer the repulsion velocity. Here we measure the velocity directly.

[10] All uncertainties reported here are 1 standard deviation combined statistical and systematic uncertainties.

[11] F. Dalfovo *et al.,* Rev. Mod. Phys. **71**, 463 (1999).

[12] D. M. Giltner, R. W. McGowan, and S. A. Lee, Phys. Rev. Lett. **75**, 2638 (1995).

[13] Y. Torii *et al.,* Phys. Rev. A **61**, 041602(R) (2000).

[14] J. Denschlag *et al.,* Science **287**, 97 (2000).

[15] The condensate was imaged by first optically pumping the atoms to the $F = 2$ ground state and then imaging the absorption of a probe beam on the $F = 2 \rightarrow F' = 3$ transition. The pulse had a 5 μs duration, $\approx$170 mW/cm^2 intensity, and was detuned 15 MHz from resonance.

[16] The momenta are not exactly $p = 0$ and $p = 2\hbar k$ because of repulsion effects that will be discussed.

[17] R. Trebino *et al.,* Rev. Sci. Instrum. **68**, 3277 (1997).

[18] The observation is consistent with the full predicted fringe contrast when we include the finite imaging resolution.

[19] We can treat the x direction independently of y and z when the wave function $\psi = fe^{i\phi(x,y,z)}$ is separable, i.e., $\phi(x,y,z) = \varphi(x) + \eta(y,z)$. Straight fringes imply this separability.

[20] Y. Castin and R. Dum, Phys. Rev. Lett. **77**, 5315 (1996).

[21] For $T_0 = 6$ ms and an interference pattern with many fringes, we found that the coefficients of third and fourth order terms are smaller than 1×10^{-5} μm^{-3} and 1×10^{-7} μm^{-4}, respectively.

[22] In practice, C includes a random phase from mirror vibrations.

[23] We use $\delta x = \frac{2\hbar k}{M}(T_2 - T_1) - x_\epsilon$ where $\frac{2\hbar k}{M} = 5.9$ cm/s is the two photon recoil velocity of sodium and x_ϵ is a small correction of the order $\delta v T_1$ due to the repulsion of the wave packets. We include the correction in our data analysis in a self-consistent manner. The correction modifies α insignificantly, but increases the final values of δv by $\approx$0.05 mm/s.

[24] V. M. Pérez-Garcia *et al.,* Phys. Rev. Lett. **77**, 5320 (1996).

[25] In fact, after the first pulse the wave packets contract because the reduced mean-field energy can no longer support the wave packet size.

[26] We also correct the fringe spacings for the contraction of the wave packets between the final interferometer pulse and when the image is taken.

[27] We assume $\delta v \ll \frac{\hbar k}{M}$, $T\omega_x \ll 1$, and harmonic motion in the trap.

[28] S. Burger *et al.,* Phys. Rev. Lett. **83**, 5198 (1999).

[29] M. R. Matthews *et al.,* Phys. Rev. Lett. **83**, 2498 (1999).

[30] K. W. Madison *et al.,* Phys. Rev. Lett. **84**, 806 (2000).

[31] A. D. Jackson, G. M. Kavoulakis, and C. J. Pethick, Phys. Rev. A **58**, 2417 (1998).